Optical Engineering

OpticalEngineering.SPIEDigitalLibrary.org

Evaluation on the capacity and outage performance of the free space optical system impaired by timing jitters over an aggregate channel

Yatian Li
Shaoai Guo
Tianwen Geng
Shuang Ma
Shijie Gao
Huibin Gao

SPIE.

Yatian Li, Shaoai Guo, Tianwen Geng, Shuang Ma, Shijie Gao, Huibin Gao, "Evaluation on the capacity and outage performance of the free space optical system impaired by timing jitters over an aggregate channel," *Opt. Eng.* **56**(7), 076108 (2017), doi: 10.1117/1.OE.56.7.076108.

Evaluation on the capacity and outage performance of the free space optical system impaired by timing jitters over an aggregate channel

Yatian Li,[a,b,*] Shaoai Guo,[c] Tianwen Geng,[a] Shuang Ma,[a] Shijie Gao,[a] and Huibin Gao[a]
[a]Chinese Academy of Sciences, Changchun Institute of Optics, Fine Mechanics and Physics, Changchun, China
[b]University of Chinese Academy of Sciences, Beijing, China
[c]Chang Guang Satellite Technology Co., Ltd., Changchun, China

Abstract. This paper proposed an analytical approach to evaluate the timing jitter's impairment to the ergodic capacity and outage performance of an on-off keying wireless optical link, where the compound channel consists of Gamma–Gamma turbulence and pointing errors. Due to the complexity in deducing ergodic capacity, the closed-form bounds are developed, as well as the asymptotic limit. Meanwhile, the Gaussian–Hermite polynomial approximation is exploited to obtain the closed-form expression of outage probability in series. It has been verified by both theoretical results and the Monte-Carlo simulations that the timing jitter leads to a restriction of the ergodic capacity, even with tremendous transmitting power. In the meantime, small timing jitters could be endurable in the analysis of outage probability, whereas the large timing jitters diverge from the lower ones. [DOI: 10.1117/1.OE.56.7.076108]

Keywords: ergodic capacity; outage probability; free space optics; timing jitter; pointing errors; Gamma–Gamma turbulence.

Paper 170507 received Apr. 5, 2017; accepted for publication Jun. 26, 2017; published online Jul. 21, 2017.

1 Introduction

Compared with the radio frequency technology, the free space optical (FSO) communication systems are rapidly gaining popularity, due to the advantages of tremendous bandwidth, secure transmission, license-free operation, etc.[1–3] Despite these strong points, there are also some inevitable challenges hampering the performance. The major one may be the turbulence, which would result in the intensity's scintillation and the phase's perturbation at the receiving end. There have already been several statistical models to characterize the turbulence, including log-normal[4] and negative exponential model,[5] where the turbulence varies from weak to strong, respectively. The classic Gamma–Gamma channel model has the ability of depicting turbulence conditions from weak to strong,[6] which is discussed in this paper. It needs to mention that some turbulence models have been developed latterly, containing but not limited to double-generalized Gamma model,[7] Mlaga model,[8] and double-Weibull model.[9] In addition to the impairment from the turbulence, the FSO system also suffers from the degradation caused by misalignment errors. The original model was proposed by Farid and Hranilovic, considering that jitters are independent identical distributed in both horizontal and vertical directions.[10] It is also the basic model of this paper. Later on, several novel models were proposed, such as Rician distribution by Ansari et al.,[11] Hoyt distribution by Sharma et al.,[12] and Beckmann distribution by AlQuwaiee.[13] It is also mentioned that literatures arguing the situation of nonzero boresight are given in Refs. 14 and 15.

This paper focused on the timing jitter's impairment to the FSO system, where the on-off keying (OOK) scheme is discussed. In the light of the simplicity to implement, the techniques of intensity modulation and direct detection (IM/DD) were proposed and widely employed originally.[16] Despite the fact of being discussed for a period of time, it still has an undiminished attraction.[17–19] As the two main parameters of this paper, both the ergodic capacity and the outage probability have been argued over the decades. The former was investigated to determine the maximum data rate that can be transmitted with an arbitrarily small bit error rate (BER) over a channel for a given average signal power,[20] and the latter was declared to evaluate the features of fading channel. In the recent works, the ergodic capacity has been studied in the relaying schemes,[21] multiple-input/single-output regimes,[22] and multiple-input multiple-output circumstances.[23] The outage probability was also further deliberated in Refs. 24 and 25.

Timing jitter is a major issue that would be mainly debated. It was proposed to quantify the impairment caused by an unsatisfactory clock in the high-speed communication system, especially with the gigabit data rates. On the basis of Ref. 26, it could be made up of the deterministic jitter (DJ) and the random jitter (RJ). The issues combing the timing jitter and FSO systems were discussed in Refs. 27 and 28. The error performance has been analyzed, where an avalanche photodiode is supplied in the receiver in the pulse position modulation (PPM) regime. The conditional BER expression of a certain timing jitter has been derived and then the average BER. However, these literatures only evaluated the performance under the circumstance of weak turbulence. Thus, our previous work elaborated the timing jitter's penalty to the symbol error rate of the PPM FSO system under Gamma–Gamma turbulence.[29] In the meantime, the misalignment errors were also taken into consideration. In

*Address all correspondence to: Yatian Li, E-mail: yt_li@ciomp.ac.cn

0091-3286/2017/$25.00 © 2017 SPIE

the FSO system with the modulation of OOK, the timing jitter could also provide an inevitable displacement from the ideal decision point, which may hamper the system's performance. To the best of the authors' knowledge, it has not been analyzed that how the timing jitter impairs the capacity of the FSO system. Motivated by these, this paper analyzes the ergodic capacity and outage probability of the FSO system with the aggregated channel, in order to measure the timing jitter's influence quantitatively. The novelties of this paper are mainly summarized as follows.

1. Compared with the existing literatures, a more generalized model of timing jitter was utilized to evaluate the influence on the performance of the FSO system, instead of the random jitter case by Refs. 27–29.
2. The impact of timing jitter is conceived as an interference to the adjacent bit. The signal-to-interference-plus-noise ratio (SINR) $\tilde{\gamma}$ is employed to appraise the performance of the system, taking the place of the signal-to-noise ratio (SNR) γ.
3. In terms of the ergodic capacity $\bar{C}$, the upper and lower bounds are deduced in the closed form. What is more, it is proved that the bounds are tight enough with low transmitting power P_t.
4. The asymptotic limit is also achieved in order to measure the ergodic capacity $\bar{C}$ with sufficiently large P_t.
5. It is formulated that the exact closed-form of outage probability P_{out} versus timing jitters.

For brevity, the remainder of this paper is organized as follows. Both the system structure and the channel model are depicted in Sec. 2, as well as the definition of the timing jitter. In Sec. 3, it is elaborated that the expressions of ergodic capacity, regarding both timing jitter and misalignment in the Gamma–Gamma turbulence. The bounds and asymptotic analysis are also illustrated. Section 4 discusses the evaluation of the outage probability. Theoretical results are further confirmed by the Monte-Carlo ones in Sec. 5. In the end, conclusions are drawn in Sec. 6.

2 System Model

2.1 *System Structure*

In this paper, a turbulence-introduced point to point (P2P) IM/DD FSO link with misalignments, which suffers from the timing jitter is considered. The structure is shown in Fig. 1. In the OOK scheme, the data $x(t)$ after modulation are represented by either the presence (on) or absence (off) at the transmitter, which is described as $x(t) \in (0, 2P_t/R_b)$. P_t and R_b stand for the average transmitting power and the data rate, respectively.

After propagating through the compound channel h expounded in Sec. 2.2, the receiver converts the lasers into electrical signals by the photo diode. With regard to the timing jitter ξ introduced in Sec. 2.3, the decision point deviates from the ideal point. As a result, the electrical signal $y(t)$ at the time t could be written as

$$y(t) = \eta \cdot h \cdot x(t-\xi) + n(t), \tag{1}$$

where η represents the photodetector responsivity. $n(t)$ denotes the equivalent noise at the receiver, which could be modeled as the additive white Gaussian noise with the variance σ_n^2.

2.2 *Channel Model*

In this paper, a composite channel h is considered, including the attenuation h_l, the turbulence fading h_a, and the pointing error loss h_p. According to the Beers–Lambert law, h_l could be derived in Eq. (2), which contains the impact of beam extinction and path loss

$$h_l = \exp(-\sigma_l \cdot z), \tag{2}$$

where σ_l stands for the attenuation factor, with the transmission path's length to be z.

h_a follows the Gamma–Gamma distribution, furnished by

$$f_{h_a}(h_a) = \frac{2(\alpha\beta)^{\frac{\alpha+\beta}{2}}}{\Gamma(\alpha)\Gamma(\beta)} h_a^{\frac{\alpha+\beta}{2}} K_{\alpha-\beta}\left(2\sqrt{\alpha\beta h_a}\right), \tag{3}$$

where $\Gamma(\cdot)$ is the Gamma function, $K_\nu(\cdot)$ denotes the ν'th-order modified Bessel function of the second kind. α and β represent the effective number of large and small scale turbulent eddies, respectively. Then, scintillation factor σ_I^2 becomes $\alpha^{-1} + \beta^{-1} + \alpha^{-1}\beta^{-1}$.

The model of pointing errors with zero boresight is discussed, as proposed in Ref. 10. It is defined that the displacements in both vertical and horizontal directions obey the independent identical Gaussian distributions with the common variance σ_s^2 at the receive plane. For an aperture

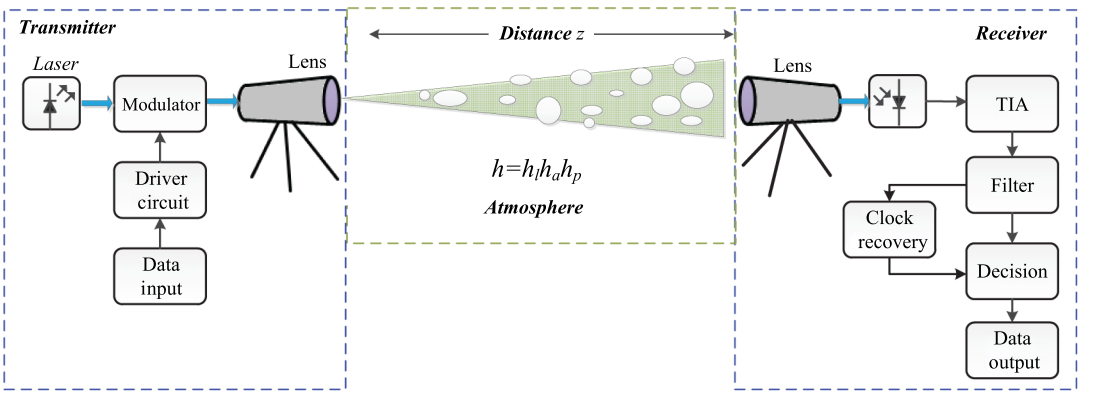

Fig. 1 System structure.

with the radius a and the beam width w_z at the distance z, the maximum fraction of the collected power is furnished by $A_0 = [\mathrm{erf}(v)]^2$, where v stands for the ratio $v = \sqrt{\pi}a/\sqrt{2}w_z$ with $\mathrm{erf}(\cdot)$ denoting the error function. Thus, the probability density function (PDF) $f_{h_p}(h_p)$ of the misalignment is shown as

$$f_{h_p}(h_p) = \frac{\rho^2}{A_0^{\rho^2}}(h_p)^{\rho^2-1}, \tag{4}$$

where $\rho = w_{zeq}/2\sigma_s$ represents the ratio between the equivalent beam radius and the displacement standard deviation (std.) σ_s. w_{zeq} could be derived by $w_{zeq} = \{w_z\sqrt{\pi}\mathrm{erf}(v)/[2v \cdot \exp(-v^2)]\}^{1/2}$. Taking the three components h_l, h_a, h_p into consideration, the PDF $f_h(h)$ is obtained by Ref. 10, which is

$$f_h(h) = \frac{\alpha\beta\rho^2}{A_0 \cdot h_l\Gamma(\alpha)\Gamma(\beta)} G_{1,3}^{3,0}\left(\frac{\alpha\beta h}{A_0 \cdot h_l}\middle| \begin{matrix}\rho^2 \\ \rho^2-1, \alpha-1, \beta-1\end{matrix}\right). \tag{5}$$

2.3 *Timing Jitter*

In a high-speed digital communication system, timing jitter could do inevitable harm to performance, especially in the case of several gigabits or even terabits per second. As shown in Fig. 2, timing jitter Δ is proposed to measure the displacement depart from the ideal clock in the time domain. It causes a skew of the decision point, which injures the performance of the whole system. In most of the literatures, the timing jitter is normalized to the unit interval (UI) for brevity, which is $\xi = \Delta/T_b$. Note that the T_b denotes the reciprocal of the bit rate in the OOK system, whereas it presents the period of the unit slot in PPM system. The latter has been analyzed in our previous work.[29]

Before depicting the classification of the jitter, the causes of the jitter should be given. The jitter could be aroused by the thermal noise, the noise of ground or power source in the circuit board, the instability of electric circuit, etc. On the basis of Ref. 26, the timing jitter can be separated into DJ and RJ at the first-stage classification. The latter could be modeled as a Gaussian variable. However, components of the former are more complicated. It could be further divided into period jitter, data-dependent jitter (DDJ), and the bounded uncorrelated jitter. Furthermore, the DDJ is made up of duty-cycle distortion and intersymbol interference. Generally speaking, RJ remains infinitely limited while it is bounded in the case of DJ. The harmonic waves representing the jitter sources could be seen in the frequency spectrum of DJ. Note that total jitter (TJ) is exploited to measure the mixture of various jitter components in actual systems.

In order to discuss the timing jitter's reduction of the performance, the distribution of ξ is illustrated. The double Dirac function is utilized to characteristic the DJ, which is[26]

$$P_{\xi,\mathrm{DJ}} = \frac{1}{2}[\delta(\xi - A) + \delta(\xi + A)], \tag{6}$$

where $\delta(\xi)$ stands for the Dirac delta function, which is the DJ's peak value. The Gaussian distribution $P_{\xi,\mathrm{RJ}}$ with the standard deviation of RJ is furnished as

$$P_{\xi,\mathrm{RJ}} = \frac{1}{\sqrt{2\pi}\sigma}\exp\left(-\frac{\xi^2}{2\sigma^2}\right). \tag{7}$$

By the composite influence of both RJ and DJ, the TJ results from the convolution of Eqs. (6) and (7) with the PDF $P_{\xi,\mathrm{TJ}}$ in Eq. (8), which could be described as a double-peaked form

$$\begin{aligned} P_{\xi,\mathrm{TJ}} &= P_{\xi,\mathrm{DJ}} * P_{\xi,\mathrm{RJ}} \\ &= \frac{1}{2\sqrt{2\pi}\sigma}\left\{\exp\left[-\frac{(\xi-A)^2}{2\sigma^2}\right] + \exp\left[-\frac{(\xi+A)^2}{2\sigma^2}\right]\right\}. \end{aligned} \tag{8}$$

Since the symmetrical characteristic of $P_{\xi,\mathrm{TJ}}$, it may be assumed that the timing jitter ξ satisfies the condition of being a positive variable as well. That is to say, the PDF P_ξ of the timing jitter ξ is ultimately formulated as

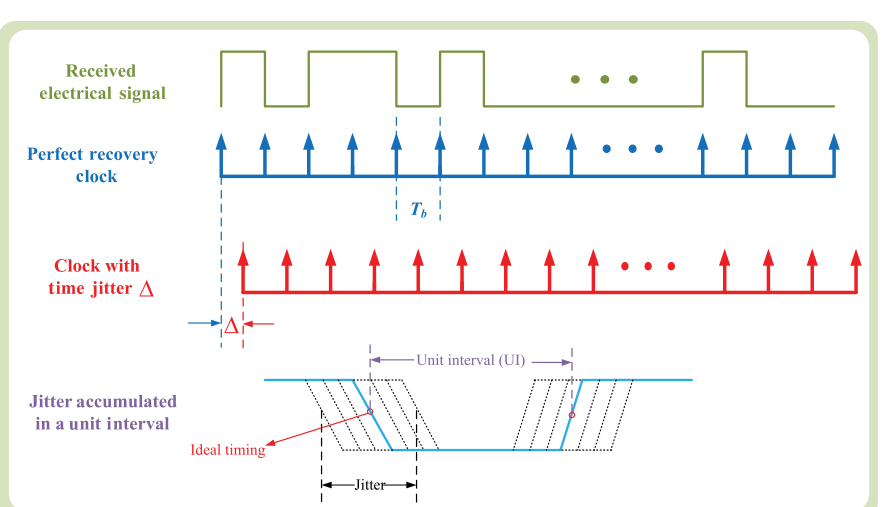

Fig. 2 The sketch of timing jitter.

$$P_\xi = \frac{1}{\sqrt{2\pi}\sigma}\left\{\exp\left[-\frac{(\xi-A)^2}{2\sigma^2}\right] + \exp\left[-\frac{(\xi+A)^2}{2\sigma^2}\right]\right\}, \quad \xi \geq 0. \tag{9}$$

3 Ergodic Capacity

As known to all, the turbulence is modeled as a slow fading channel, since the coherent time stays in the order of milliseconds while the magnitude of the transmission rate R_b is always gigabit. Beyond that, enormous interleavers should be utilized in order to achieve independent fading samples in consecutive symbol intervals, which is not realistic in the real-time FSO system. According to Shannon,[20] ergodic capacity describes the upper limit of the data rate under the condition of arbitrary small BER. In this paper, the purpose of arguing the ergodic capacity is to study the timing jitter's penalty on the maximum data rate quantitatively. In regard to the ideal system, which is free of the timing jitter, the average power of every bit is deduced as $\eta^2 P_t^2 h^2 / R_b$. It is evident to get that the SNR is equal to $\gamma \triangleq \eta^2 P_t^2 h^2 / R_b \sigma_n^2$. However, due to the timing jitter ξ, only the portion $(1-\xi)\eta^2 P_t^2 h^2 / R_b$ contributes to the signal power. What is more, the rest portion of the power $\xi\eta^2 P_t^2 h^2 / R_b$ results in the interference of the next contiguous bit. As a result, it is more rational to apply the SINR $\tilde{\gamma}$ in deriving the ergodic capacity rather than the traditional SNR. The ergodic capacity follows the expression given by

$$C = \log_2(1+\tilde{\gamma}) = \log_2\left[1 + \frac{(1-\xi)P_t^2\eta^2h^2}{R_b\sigma_n^2 + \xi P_t^2\eta^2h^2}\right], \tag{10}$$

where the receiver end's SINR $\tilde{\gamma}$ is equal to $\tilde{\gamma} = \Delta \frac{(1-\xi)P_t^2\eta^2h^2}{R_b\sigma_n^2+\xi P_t^2\eta^2h^2} = \frac{(1-\xi)\gamma}{1+\xi\gamma}$. It is defined that the expectation of ergodic capacity is $\bar{C} = \mathbb{E}[C]$, which is calculated by

$$\begin{aligned}\bar{C} &= \int_{-\infty}^{\infty}\int_0^{\infty} \log_2\left[1 + \frac{(1-\xi)P_t^2\eta^2h^2}{R_b\sigma_n^2 + \xi P_t^2\eta^2h^2}\right] f_h(h) f_\xi(\xi)\cdot \mathrm{d}h \cdot \mathrm{d}\xi \\ &= \int_0^{\infty}\int_0^{\infty} \log_2\left[1 + \frac{(1-\xi)P_t^2\eta^2h^2}{R_b\sigma_n^2 + \xi P_t^2\eta^2h^2}\right] \frac{\alpha\beta\eta^2}{h_l A_0\Gamma(\alpha)\Gamma(\beta)} \\ &\quad \times G_{1,3}^{3,0}\left(\frac{\alpha\beta h}{h_l A_0}\middle| \begin{matrix}\eta^2 \\ \eta^2-1, \alpha-1, \beta-1\end{matrix}\right) \\ &\quad \cdot \frac{1}{\sigma\sqrt{2\pi}}\left\{\exp\left[-\frac{(\xi-A)^2}{2\sigma^2}\right] + \exp\left[-\frac{(\xi+A)^2}{2\sigma^2}\right]\right\}\mathrm{d}h \cdot \mathrm{d}\xi.\end{aligned} \tag{11}$$

However, to the best of the authors' knowledge, Eq. (11) is too sophisticated to be simplified. Thus, motivated by Refs. 30 and 31, the approximate results could be derived by its upper and lower bounds, which will be illustrated in Sec. 3.1 and Sec. 3.2, respectively.

3.1 *Derivation of the Upper Bound*

The procedure of obtaining the upper bound C_{up} could be divided into two conditions with SINR $\tilde{\gamma} \leq 1$ and $\tilde{\gamma} > 1$. To begin with, suppose $\tilde{\gamma}$ to be smaller than 1. In this way, $R_b\sigma_n^2$ dominates the value of the whole denominator $R_b\sigma_n^2 + \xi P_t^2\eta^2h^2$. As a result, the upper bound becomes

$$\begin{aligned}\bar{C}_{\mathrm{up}} &= E[C_{\mathrm{up}}] = E\left\{\log_2\left[1 + \frac{(1-\xi)P_t^2\eta^2h^2}{R_b\sigma_n^2}\right]\right\}, \quad \tilde{\gamma} \leq 1 \\ &= \int_0^{\infty} C_{\mathrm{up}}|\xi \cdot \frac{1}{\sigma\sqrt{2\pi}}\left\{\exp\left[-\frac{(\xi-A)^2}{2\sigma^2}\right] \right. \\ &\quad \left. + \exp\left[-\frac{(\xi+A)^2}{2\sigma^2}\right]\right\}\mathrm{d}\xi,\end{aligned} \tag{12}$$

where the conditional expectation $C_{\mathrm{up}}|\xi$ is an integral of h, representing

$$\begin{aligned}C_{\mathrm{up}}|\xi = \int_0^{\infty} &\log_2\left[1 + \frac{(1-\xi)P_t^2\eta^2h^2}{R_b\sigma_n^2}\right] \cdot \frac{\alpha\beta\eta^2}{h_l A_0\Gamma(\alpha)\Gamma(\beta)} \\ &\cdot G_{1,3}^{3,0}\left(\frac{\alpha\beta h}{h_l A_0}\middle| \begin{matrix}\rho^2 \\ \rho^2-1, \alpha-1, \beta-1\end{matrix}\right)\mathrm{d}h.\end{aligned} \tag{13}$$

Seeing that $\log(1+\tilde{\gamma})$ could be transformed into Meijer'G function $G_{2,2}^{1,2}\left(\tilde{\gamma}\middle| \begin{matrix}1,1 \\ 1,0\end{matrix}\right)$, $C_{\mathrm{up}}|\xi$ satisfies the form that $\int_0^{\infty} G_{u,v}^{s,t}\left[\varphi x\middle| \begin{matrix}\mathbf{(c}_u\mathbf{)} \\ \mathbf{(d}_u\mathbf{)}\end{matrix}\right] \cdot G_{p,q}^{m,n}\left[\omega x^2\middle| \begin{matrix}\mathbf{(a}_u\mathbf{)} \\ \mathbf{(b}_u\mathbf{)}\end{matrix}\right] \cdot \mathrm{d}x$. Thanks to Eq. (8) from Ref. 32, it would be further reduced to

$$\begin{aligned}C_{\mathrm{up}}|\xi &= \int_0^{\infty} G_{2,2}^{1,2}\left[\frac{2(1-\xi)P_t^2R^2}{R_b\sigma_n^2}h^2\middle| \begin{matrix}1,1 \\ 1,0\end{matrix}\right] \\ &\quad \cdot \frac{\alpha\beta\eta^2}{h_l A_0\Gamma(\alpha)\Gamma(\beta)} G_{1,3}^{3,0}\left(\frac{\alpha\beta h}{h_l A_0}\middle| \begin{matrix}\rho^2 \\ \rho^2-1, \alpha-1, \beta-1\end{matrix}\right)\cdot \mathrm{d}h \\ &= \frac{\rho^2}{2\pi\Gamma(\alpha)\Gamma(\beta)} G_{8,4}^{1,8} \\ &\quad \times\left[\frac{32(1-\xi P_t^2R^2)h_l A_0}{R_b\sigma_n^2\alpha^2\beta^2}\middle| \begin{matrix}1, \frac{1-\rho^2}{2}, \frac{2-\rho^2}{2}, \frac{1-\alpha}{2}, \frac{2-\alpha}{2}, \frac{1-\beta}{2}, \frac{2-\beta}{2}, 0 \\ 1, -\frac{\rho^2}{2}, \frac{1-\rho^2}{2}, 0\end{matrix}\right].\end{aligned} \tag{14}$$

In this light, it is depicted that $\bar{C}_{\mathrm{up}}$ results in the form of $\int_0^{+\infty} g(\zeta)\cdot e^{-\zeta^2}\mathrm{d}\zeta$. With the help of Gaussian–Hermite polynomials, the closed form of $\bar{C}_{\mathrm{up}}$ is given as

$$\begin{aligned}\bar{C}_{\mathrm{up}} &= \frac{\rho^2}{2\pi^{3/2}\Gamma(\alpha)\Gamma(\beta)} \sum_{i=0}^{N}\sum_{\substack{j=-1 \\ j\neq 0}}^{1} w_i \\ &\quad \cdot \mathbf{G}_{8,4}^{1,8}\left\{\frac{32\left[1 - \left(\sqrt{2}\sigma\zeta_i + jA\right)P_t^2\eta^2\right]h_l A_0}{R_b\sigma_n^2\alpha^2\beta^2}\right\}, \quad \tilde{\gamma} \leq 1,\end{aligned} \tag{15}$$

where $\mathbf{G}_{8,4}^{1,8}(\cdot)$ is short for $G_{8,4}^{1,8}\left(\cdot\middle| \begin{matrix}1, \frac{1-\rho^2}{2}, \frac{2-\rho^2}{2}, \frac{1-\alpha}{2}, \frac{2-\alpha}{2}, \frac{1-\beta}{2}, \frac{2-\beta}{2}, 0 \\ 1, -\frac{\rho^2}{2}, \frac{1-\rho^2}{2}, 0\end{matrix}\right)$. w_i and ζ_i represent the roots and the weights of i'th-order Hermite polynomials, respectively.

In the condition that $\tilde{\gamma} \geq 1$, the ergodic capacity C's upper bound C_{up} could be derived by reducing the identical value $\xi P_t^2\eta^2h^2$ in both the denominator and the numerator, which is

$$C_{\mathrm{up}} = \log_2\left[1+\frac{(1-\xi)P_t^2\eta^2h^2}{R_b\sigma_n^2+\xi P_t^2\eta^2h^2}\right] \le \log_2\left[1+\frac{(1-2\xi)P_t^2\eta^2h^2}{R_b\sigma_n^2}\right], \quad \tilde{\gamma}>1. \tag{16}$$

In the similar method from Eqs. (12)–(16), the expectation $\bar{C}_{\mathrm{up}}$ is obtained as

$$\bar{C}_{\mathrm{up}} = \frac{\rho^2}{2\pi^{3/2}\Gamma(\alpha)\Gamma(\beta)}\sum_{i=0}^{N}\sum_{\substack{j=-1\\ j\neq 0}}^{1} w_i \cdot \mathbf{G}_{8,4}^{1,8}\left\{\frac{32\left[1-\left(2\sqrt{2}\sigma\zeta_i+2jA\right)P_t^2\eta^2\right]h_lA_0}{R_b\sigma_n^2\alpha^2\beta^2}\right\}, \quad \tilde{\gamma}>1. \tag{17}$$

To sum up, the upper bounds $\bar{C}_{\mathrm{up}}$ could be summarized from Eqs. (15) and (17), which is

$$\bar{C}_{\mathrm{up}} = \frac{\rho^2}{2\pi^{3/2}\Gamma(\alpha)\Gamma(\beta)}\sum_{i=0}^{N}\sum_{\substack{j=-1\\ j\neq 0}}^{1} w_i \times \cdot \mathbf{G}_{8,4}^{1,8}\left\{\frac{32\left[1-\mu(\tilde{\gamma})(\sqrt{2}\sigma\zeta_i+jA)P_t^2\eta^2\right]h_lA_0}{R_b\sigma_n^2\alpha^2\beta^2}\right\}, \tag{18}$$

where the coefficient $\mu(\tilde{\gamma})$ is a piecewise function, given as $\mu(\tilde{\gamma}) = \begin{cases} 1, & \tilde{\gamma}\le 1 \\ 2, & \tilde{\gamma}>1 \end{cases}$.

$\delta_{\mathrm{up}} = \bar{C}_{\mathrm{up}} - \bar{C}$ is introduced to measure how tight the upper bound is. Since there is no closed form of $\bar{C}$, this paper only analyzes the situation with small SNR γ. In that case, δ_{up} could be proved to be tight enough. The rigorous proof is given as

$$\delta_{\mathrm{up}} = \frac{1}{\ln 2}\int_{-\infty}^{\infty}\int_{0}^{\infty}\ln\left[1+\frac{\xi(1-\xi)\gamma^2}{1+\gamma}\right]f_h(h)f_\xi(\xi)\cdot \mathrm{d}h\cdot \mathrm{d}\xi. \tag{19}$$

The $\xi(1-\xi)\gamma^2$ is assumed to be an infinitesimal item relative to γ. Let alone $1+\gamma$, because it is a higher order item of γ. Thus, the upper bound is tight enough with small SNR, which will be found in Fig. 3.

3.2 *Derivation of the Lower Bound*

With the help of the Jensen inequality, the lower bound C_{low} of the ergodic capacity could be deduced succinctly. It is noted that the premise of Jensen inequality is to ensure the expression of Eq. (10) is concave or convex.

Lemma 1. Assume $f(x,y)$ to be a function of two variables (x,y) with continuous second-order partial derivative, whose Hessian matrix $\mathbf{H}_C$ satisfying $|\mathbf{H}_C|\ge 0$ (but not always equal to zero). It would be predicated as a concave function if either f''_{xx} or f''_{yy} is positive. Oppositely, it is a convex function if either f''_{xx} or f''_{yy} is smaller than 0. Note that $|\cdot|$ means the determinant $\det(\cdot)$, and f''_{xx}, f''_{yy}, and f''_{xy} stand for the partial derivative of second order. However, the concavity or convexity of the function $f(x,y)$ still remains uncertain, when $|\mathbf{H}_C|<0$.

Proof. For the sake of the limited length, refer to Appendix A.

In the light of Lemma 1, Eq. (10) could be written as the form with the independent variables (ξ,h). The Hessian matrix $\mathbf{H}_C$ could be derived as

$$\mathbf{H}_C = \begin{bmatrix} C''_{\xi\xi} & C''_{\xi h} \\ C''_{\xi h} & C''_{hh}\end{bmatrix} = \begin{Bmatrix} \frac{h^4P_t^4\eta^4}{(R_b\sigma_n^2+\xi P_t^2\eta^2h^2)^2} & \frac{-2\ hP_t^2\eta^2\sigma_n^2}{(R_b\sigma_n^2+\xi P_t^2\eta^2h^2)^2} \\ \frac{-2\ hP_t^2\eta^2\sigma_n^2}{(R_b\sigma_n^2+\xi P_t^2\eta^2h^2)^2} & \frac{2(-1+\xi)[-P_t^2\eta^2R_b\sigma_n^6+3\xi h^4P_t^6\eta^6R_b\sigma_n^2+h^2P_t^4\eta^4(1+\xi)]}{(P_t^2\eta^2h^2+R_b\sigma_n^2)^2(R_b\sigma_n^2+\xi P_t^2\eta^2h^2)^2}\end{Bmatrix}. \tag{20}$$

Conceiving the fact that $C''_{\xi\xi}$ has the square form, it is obvious to see that $C''_{\xi\xi}\ge 0$. As a result, it is a requisite condition that C''_{hh} is positive, in order to ensure that $|\mathbf{H}_C| = C''_{\xi\xi}\cdot C''_{hh} - C''^{\,2}_{\xi h}\ge 0$. Otherwise, $|\mathbf{H}_C|$ is determined to be less than 0. After some algebra (the details are given in Appendix B), Eq. (10) is derived to be concave under the circumstance that $0<h<\sqrt{R_b\sigma_n^2/3P_t^2\eta^2}$.

On this occasion, the lower bound is given as Eq. (21), thanks to the Jensen inequality, which is

$$\bar{C}_{\mathrm{low}} = \frac{1}{\ln 2}\ln\left\{1+\frac{(1-\mathbb{E}[\xi])P_t^2\eta^2\mathbb{E}[h^2]}{R_b\sigma_n^2+\mathbb{E}[\xi]P_t^2\eta^2\mathbb{E}[h^2]}\right\}, \tag{21}$$

where the expectation $\mathbb{E}[\xi]$ is equal to $\sqrt{\frac{2}{\pi}}\sigma\cdot\exp(-\frac{A^2}{2\sigma^2})+A\cdot\mathrm{erf}(-\frac{A}{\sqrt{2}\sigma})$. Owing to the independence of h_l, h_a, h_p, the expectation $\mathbb{E}[h^2]$ could be obtained from $\mathbb{E}[h_l^2]\mathbb{E}[h_a^2]\mathbb{E}[h_p^2]$. Then, Eq. (21) could be further simplified as

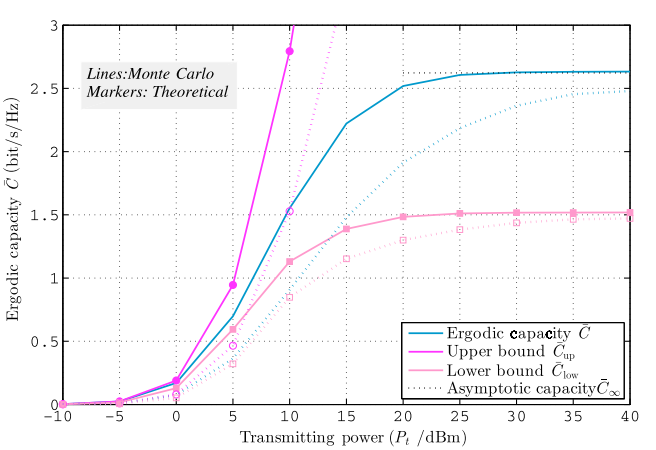

Fig. 3 The ergodic capacity $\bar{C}$ versus transmitting power P_t and its bounds with $\alpha=4$, $\beta=2$ (in solid lines and filled markers) and $\alpha=2$, $\beta=1$ (in dotted lines and hollow markers).

$$\bar{C}_{\text{low}} = \frac{1}{\ln 2} \ln\left\{\frac{(1+\rho^2)^2 R_b\sigma_n^2 + P_t^2\eta^2 h_l^2 A_0^2\rho^4\sigma_I^2}{(1+\rho^2)^2\sigma_n^2 + \left[\sqrt{\frac{2}{\pi}}\sigma\cdot\exp\left(-\frac{A^2}{2\sigma^2}\right) + A\cdot\text{erf}\left(-\frac{A}{\sqrt{2}\sigma}\right)\right]P_t^2\eta^2 h_l^2 A_0^2\rho^4\sigma_I^2}\right\}, \tag{22}$$

where scintillation factor σ_I^2 is equal to $\alpha^{-1}+\beta^{-1}+\alpha^{-1}\beta^{-1}$.

Taking $h > \sqrt{R_b\sigma_n^2/3P_t^2\eta^2}$ into consideration, the concavity and convexity would remain uncertain. That is to say, the Jensen inequality becomes disabled. However, it is remarked that the simulation still proves that Eq. (22) is lower than Eq. (10), which will be found in Fig. 3. Therefore, it is suitable to define Eq. (22) as the lower bound of Eq. (10).

In order to elaborate how tight the lower bound $\bar{C}_{\text{low}}$ is, δ_{low} is introduced, which is defined as $\delta_{\text{low}} = \bar{C} - \bar{C}_{\text{low}}$. It is discovered that δ_{low} approaches zero with lower $\tilde{\gamma}$. It is evident to simplify $\bar{C}$ by the approximation of $\log(1+\tilde{\gamma}) \sim \tilde{\gamma}$. Since the independence of ξ and h, $\bar{C}$ could be calculated by $\mathbb{E}[h^2]$ and $\mathbb{E}[\xi]$, which is $\bar{C} \sim \frac{1}{\ln 2}\mathbb{E}\left[\frac{(1-\xi)P_t^2\eta^2h^2}{R_b\sigma_n^2+\xi P_t^2\eta^2h^2}\right]$. In the similar way, $\bar{C}_{\text{low}}$ becomes $\frac{1}{\ln 2}\frac{(1-\mathbb{E}[\xi])P_t^2\eta^2\mathbb{E}[h^2]}{R_b\sigma_n^2+\mathbb{E}[\xi]P_t^2\eta^2\mathbb{E}[h^2]}$, which confirms the approximate expression of $\frac{1}{\ln 2}\frac{(1-\mathbb{E}[\xi])P_t^2\eta^2\mathbb{E}[h^2]}{R_b\sigma_n^2+\mathbb{E}[\xi]P_t^2\eta^2\mathbb{E}[h^2]}$. Due to the distribution of ξ, any arbitrary small $\tilde{\gamma}$ could be equivalent to say $\gamma \to 0$. That is to say, the lower bound maintain tight when γ is small.

3.3 *Asymptotic Analysis*

In the timing-jitter-free FSO link, it is apparent that the ergodic capacity enhances with the higher SNR γ. There seems to be no boundary that restricts the capacity. However, the timing jitter ξ provides a constraint on the upper bound of ergodic capacity, even with enormous SNR γ, which is defined as the asymptotic capacity in this paper. Pondering the expression of Eq. (10), it could be reformulated with sufficient large SNR γ. The noise $R_b\sigma_n^2$ may be neglected, compared to the interference $\xi P_t^2\eta^2h^2$, the SINR $\tilde{\gamma}$ could be reduced to

$$\lim_{\gamma\to\infty}\tilde{\gamma} = \lim_{\gamma\to\infty}\frac{(1-\xi)\gamma}{1+\xi\gamma} = \lim_{\gamma\to\infty}\frac{(1-\xi)}{1/\gamma+\xi} = \frac{1-\xi}{\xi}. \tag{23}$$

From Eq. (23), it is manifested to conclude that the timing jitter ξ affects the maximum of the SINR $\tilde{\gamma}$, rather than the infinite case of SNR γ in the ideal system with ideal clocking. This gives a hint that the timing jitter may set a restriction on the capacity, even when the SNR γ is infinitely great. Thus, the asymptotic capacity $\bar{C}_\infty \triangleq \lim_{\gamma\to\infty}\bar{C}$ is introduced, which is calculated by

$$\begin{aligned}\bar{C}_\infty &= \int_0^\infty \log_2\left(1+\frac{1-\xi}{\xi}\right)\cdot f_\xi(\xi)\text{d}\xi\cdot\int_{-\infty}^{\infty} f_h(h)\text{d}h \\ &= \int_0^\infty \log_2\left(1+\frac{1-\xi}{\xi}\right)\cdot\frac{1}{\sigma\sqrt{2\pi}}\left\{\exp\left[-\frac{(\xi-A)^2}{2\sigma^2}\right]\right. \\ &\quad \left.+\exp\left[-\frac{(\xi+A)^2}{2\sigma^2}\right]\right\}\text{d}\xi \\ &= \mathbb{E}[-\log_2\xi].\end{aligned} \tag{24}$$

After some tedious but straightforward algebra, the closed form of $\bar{C}_\infty$ is furnished by

$$\begin{aligned}\bar{C}_\infty &= 2\log_2\sigma \\ &\quad -\sum_{\substack{j=-1\\ j\neq 0}}^{1}\frac{1}{4}e^{-\frac{A^2}{2}}\left\{\sqrt{2\pi}e^{-\frac{A^2}{2}}\left[{}_1F_1^{(1,0,0)}\left(0,\frac{1}{2},-\frac{A^2}{2}\right)\right.\right. \\ &\quad \left.+(\gamma-\ln 2)\text{erfc}\left(\frac{jA}{\sqrt{2}}\right)+\ln 4\right] \\ &\quad \left.-2jA\cdot{}_1F_1^{(1,0,0)}\left(0,\frac{3}{2},\frac{A^2}{2}\right)\right\},\end{aligned} \tag{25}$$

where γ denotes the Euler's constant, approximated by 0.577. ${}_1F_1^{(1,0,0)}$ is the Kummer confluent hypergeometric function. $\text{erfc}(\cdot)$ means the complementary error function.

4 Outage Performance Analysis

According to the Shannon theory,[20] the outage event occurs when the data rate R is greater than the ergodic capacity C. In this case, the transmitted codewords are not able to be reliably decoded at the receiver and the outage probability is defined as $P_{\text{out}} = \Pr[R > C]$. Conceiving the expression of C in Eq. (10), the threshold of SINR $\tilde{\gamma}_{\text{th}}$ is supposed to be $\tilde{\gamma}_{\text{th}} = 2^{C_{\text{th}}} - 1$. Thus, the outage probability P_{out} is obtained as the expectation of $\mathbb{E}_\xi[\Pr(\tilde{\gamma} < \tilde{\gamma}_{th})]$. Owing to the independence of ξ and h, P_{out} could be derived by the Bayes equation

$$\begin{aligned}P_{\text{out}} = \int_0^\infty P_{\text{out}}\Big|\xi\cdot\frac{1}{\sigma\sqrt{2\pi}}\left\{\exp\left[-\frac{(\xi-A)^2}{2\sigma^2}\right]\right. \\ \left.+\exp\left[-\frac{(\xi+A)^2}{2\sigma^2}\right]\right\}\text{d}\xi,\end{aligned} \tag{26}$$

where the conditional probability $P_{\text{out}}|\xi$ denotes the expectation of $\mathbb{E}_h[\Pr(\tilde{\gamma} < \tilde{\gamma}_{th})]$ with a certain timing jitter ξ, which is

$$P_{\text{out}}|\xi = \Pr(\tilde{\gamma} < \tilde{\gamma}_{\text{th}}) = \Pr\left\{h^2 \le \frac{\tilde{\gamma}_{\text{th}}R_b\sigma_n^2}{[1-\xi(\tilde{\gamma}_{\text{th}}+1)]P_t^2\eta^2}\right\}. \tag{27}$$

Before acquiring the result of $P_{\text{out}}|\xi$, it is imperative to explore the cumulative density function (CDF) of h^2. It is assumed that $\tilde{h}$ stands for h^2 for brevity. Then, the CDF $F_{h^2}(\tilde{h})$ of h^2 could be formulated from Eq. (5)

$$F_{h^2}(\tilde{h}) = \frac{\eta^2}{\Gamma(\alpha)\Gamma(\beta)}G_{2,4}^{3,1}\left(\frac{\alpha\beta}{A_0h_l}\sqrt{\tilde{h}}\,\middle|\,\begin{matrix}1,\rho^2+1\\ \rho^2,\alpha,\beta,0\end{matrix}\right). \tag{28}$$

As a result, we have the expression of simplified $P_{\text{out}}|\xi$

$$P_{\text{out}}|\xi=\frac{\rho^2}{\Gamma(\alpha)\Gamma(\beta)}G_{2,4}^{3,1}\left\{\frac{\alpha\beta}{A_0h_l}\frac{(\tilde{\gamma}_{th}\cdot R_b)^{1/2}\sigma_n}{[1-\xi(\tilde{\gamma}_{th}+1)]^{1/2}P_t\eta}\middle|\begin{matrix}1,\rho^2+1\\ \rho^2,\alpha,\beta,0\end{matrix}\right\}. \tag{29}$$

By substituting Eq. (29) into Eq. (26), the closed-form of outage probability P_{out} could also be derived by the Gaussian–Hermite polynomials, shown as

$$P_{\text{out}}=\frac{\rho^2}{\Gamma(\alpha)\Gamma(\beta)\pi^{1/2}}\sum_{i=0}^{N}\sum_{\substack{j=-1\\ j\neq 0}}^{1}w_iG_{2,4}^{3,1}\left\{\frac{\alpha\beta}{A_0h_l}\frac{(\tilde{\gamma}_{\text{th}}\cdot R_b)^{1/2}\sigma_n}{\left[1-(\sqrt{2}\sigma\zeta_i+jA)(\tilde{\gamma}_{\text{th}}+1)\right]^{1/2}P_t\eta}\middle|\begin{matrix}1,\rho^2+1\\ \rho^2,\alpha,\beta,0\end{matrix}\right\}, \tag{30}$$

where w_i and ζ_i denote the roots and the weights of i'th-order Hermite polynomials, respectively.

5 Numeric Results

In this section, the numeric results of the ergodic capacity and outage performance, respectively are discussed. The parameters adopted in the simulation are furnished by Table 1. As a whole, the equations derived above are well validated by the Monte-Carlo simulations, which could be derived from the figures below. For convenience, it is assumed that the word "simulation" is short for the Monte-Carlo simulation.

Figure 3 shows how the ergodic capacity $\bar{C}$ changes versus transmitting power P_t under different turbulence conditions as well as its upper and lower bounds when the timing jitter consists of $A=0.2$, $\sigma_s=0.2$. It is noted that the Monto-Carlo results are depicted in the form of lines, with the theoretical ones in discrete markers. It is confirmed that the accuracy of both the bounds in Eqs. (18) and (22) and the asymptotic results in Eq. (25). What is more, the bounds remain rather tight with lower transmitting power P_t, as analyzed in Sec. 3. Meanwhile, the asymptotic analysis is universal, regarding different turbulent channels. As it also ought to be, the ergodic capacity increases with the transmitting power. However, it is remarked that there is a reduction in the slope of ergodic capacity $\bar{C}$, which could be analyzed as follows. With lower transmitting power P_t, it could be neglected that the interference caused by the timing jitter, compared to the noise σ_n^2. In that case, SINR $\tilde{\gamma}$ is mainly determined by the noise σ_n^2. But with the growth of transmitting power, the interference dominates the SINR $\tilde{\gamma}$ gradually, which does more harm to the large P_t conditions.

Figure 4 shows how the ergodic capacity $\bar{C}$ changes with various distance z. In the meanwhile, the case of different σ_s is also depicted. It is apparent to see that there is a decrease in ergodic capacity $\bar{C}$, when the pointing error's std. σ_s becomes larger. It is noted that the asymptotic limit is a certain value, which is not altered with the distance z and pointing error's std. σ_s. The reasons could be found from Eq. (25) that the asymptotic limit is only influenced by the timing jitter's parameters $A=0.2$, $\sigma=0.2$. The conclusion could be drawn that the timing jitter sets a main handcuff on the ergodic capacity $\bar{C}$.

In order to discuss the system's result with different timing jitters, Fig. 5 shows the simulation analyses of the ergodic capacity $\bar{C}$ against various timing jitters. It is revealed that there is only a little distinction with different timing jitters in the case of small transmitting power. Meanwhile, it is depicted that the RJ remains an impairment to the ergodic capacity even under the circumstance of no DJ, i.e., $A=0$, which is illustrated in our previous work. However, when A is larger than one tenth of a UI, the RJ brings only a little distinguish on the capacity. That is to say, the DJ mainly

Table 1 Parameters in Monte-Carlo simulations.

Parameters	Value
Responsivity η	0.8 A/W
Propagation distance z	1 km
Receiving aperture a	0.1 m
Corresponding beam radius w_z at 1 km	2.5 m
Corresponding misalignment jitter standard deviation σ_s	0.2 m
Atmospheric attenuation coefficient σ	0.44 dB/km
Noise standard deviation σ_n	10^{-7} A/Hz
Effective number of large eddies α	4
Effective number of small eddies β	2
Wavelength λ	1550 nm
Data rate R_b	10 Gbps
SINR threshold $\tilde{\gamma}_{\text{th}}$	−20 dBm

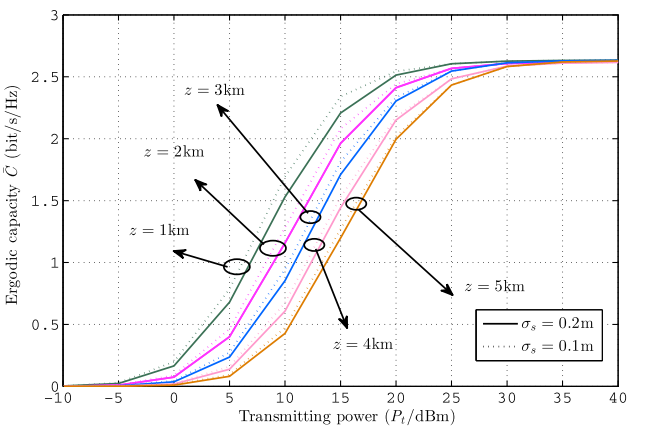

Fig. 4 The ergodic capacity $\bar{C}$ versus distance $z=1,2,3,4,5$ km with timing jitter $A=0.2$, $\sigma=0.2$.

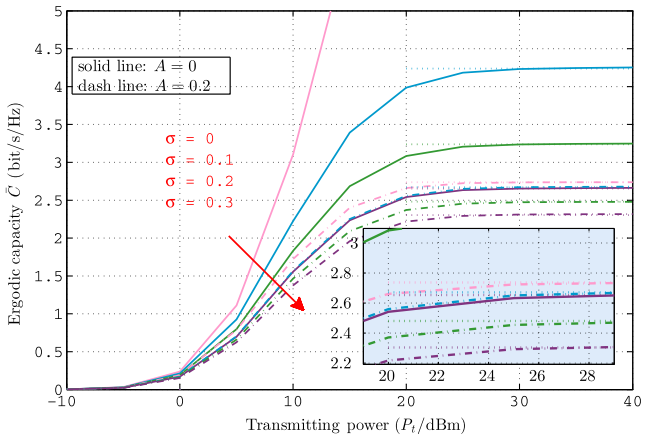

Fig. 5 The ergodic capacity $\bar{C}$ against timing jitters with $A = 0$ (in solid lines) and $A = 0.2$ (in dash-dotted lines).

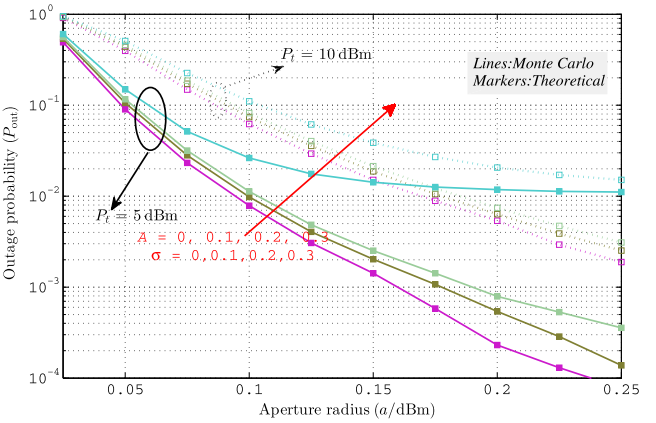

Fig. 7 The outage probability P_{out} versus the aperture radius a the with $P_t = 10$ dBm (in solid lines and filled markers) and $P_t = 5$ dBm (in dash-dotted lines and hollow markers).

injures the system's performance when it is large. It is also noted that the slopes of the curves vary with the similar trends, which results from the similar reasons in Fig. 3.

The evolutions of outage performance are furnished after the ergodic capacity analyses. As shown in Fig. 6, the outage probability P_{out} increases with the larger timing jitter. It is manifested that the timing jitter contributes to an error floor to P_{out}. In this regard, it is obtained that the timing jitter is tolerant when DJ's peak value A is smaller than 0.2 and the variance σ^2 of the RJ is no more than 0.04. In this case, the slopes of the curves are found nearly the same. In other words, it is indicated that the small timing jitter leads to a passive gain in the SINR, which depicts a translation toward the negative direction, shown in Fig. 6. However, there will be an increasing diverge in the condition of large timing jitters, e.g., $A = 0.3$, $\sigma = 0.3$. Note that even small timing jitter could bring about the limit of the SINR even with enormous transmitting power, which has been analyzed in Sec. 3.3 and verified by Fig. 5. It seems to be contrary to the results in Fig. 6, which is explained below. In a word, the small timing jitter contributes to an upper limit of the SINR, whereas P_{out} focuses on the SINR lower than the threshold $\tilde{\gamma}_{\text{th}}$, describing the timing jitter's influence on the disqualified SINRs. As it

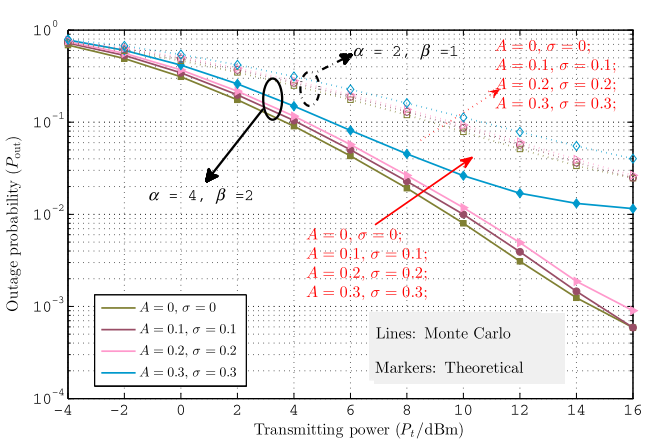

Fig. 6 The outage probability P_{out} against transmitting power P_t with $\alpha = 4$, $\beta = 2$ (in solid lines and filled markers) and $\alpha = 2$, $\beta = 1$ (in dash-dotted lines and hollow markers).

is also discovered in Fig. 6, the timing jitter does more harm to the weak turbulence links than stronger ones.

As one can see in Fig. 7, the outage probability P_{out} is depicted as a function of aperture radius a. The transmitting power is supposed to be 10 dBm. It is discovered that the outage performance could be ameliorated with the increase of the aperture radius a until a bottleneck appears. Definitely, the larger the aperture radius is, the more energy would be collected in the receiver. In addition, the effect of aperture averaging caused by greater aperture also mitigates the fluctuation of the receiving power. Although the growth of a contributes to the increment on the SINR, the asymptotic value of SINR still exists, as discussed before. It follows the similar reasons in the case of raising the transmitting power. From Fig. 7, it is also derived that the larger jitter will lead to a dispersion from the other curves depicting the endurable jitters, i.e., $A \leq 0.2$, $\sigma \leq 0.2$. As a whole, increasing the aperture at the receiving end is supposed to be an effective mean to fight against the small or moderate timing jitters.

6 Conclusion

In this paper, the ergodic capacity and the outage probability of the OOK-FSO system impaired by timing jitters, where the aggregated channel contains the attenuation, Gamma–Gamma turbulence, and misalignment losses is discussed. This paper evaluated the potential maximum rate by the ergodic capacity; and the theoretical bounds and the asymptotic limit are obtained. It is discovered that the bounds could be rather tight with lower transmitting powers. It is also derived that the timing jitter introduces an inevitable confine of the capacity, no matter how large the transmitting power is. There would still be an asymptotic limit even in the infinitely small timing jitter.

In terms of the outage probability, it is evaluated that the small timing jitters is tolerant, whereas a large timing jitter will result in an higher error floor, which is apart from the lower ones. What is more, it is revealed that a larger aperture helps to mitigate the penalty of the timing jitters. We hope this paper could be a user guide that helps to determine the target restrictions for the timing jitter, when proposing the indexes during the system design.

Appendix A

In this appendix, only the circumstance of concave function is analyzed. The condition of convexity is the similar case with the minor changes on the sign. Before proving Lemma 1, the conception of convex domain is illustrated.

Definition 1. Assume that any arbitrary two points $P(x_1, x_2)$ and $P(x_1', x_2')$ in the domain $\mathbf{D}$ in the two-dimensional space, which means that $P(x_1, x_2) \in \mathbf{D}$, $P(x_1', x_2') \in \mathbf{D}$. $\mathbf{D}$ is defined as convex domain when satisfying the condition that the point $P[x_1 + \theta(x_1' - x_1), x_2 + \theta(x_2' - x_2)]$ still belongs to the domain for any positive θ.

The proof of Lemma 1 is furnished as below, which is based on the definition of the concave function or concave one.

Proof. Suppose that $f(x, y)$ represents a function with the convex domain $\mathbf{D}$. It is also assumed that the two different points $P_1(x_1, y_1)$ and $P_2(x_2, y_2)$ are geared to domain $\mathbf{D}$ with the midpoint $P_0(x_0, y_0) = P_0(\frac{x_1+x_2}{2}, \frac{y_1+y_2}{2})$. Thanks to the Taylor's formula of second order, the function $f(x, y)$ could be expanded as

$$\begin{aligned} f(P_1) &= f(P_0) + (x_1 - x_0)f_x'(P_0) + (y_1 - y_0)f_y'(P_0) + o_1/2 \\ f(P_2) &= f(P_0) + (x_2 - x_0)f_x'(P_0) + (y_2 - y_0)f_y'(P_0) + o_2/2, \end{aligned} \tag{31}$$

where o_1 and o_2 stand for the second-order items in Taylor series. Therefore, it is evident to obtain that

$$\frac{f(P_1) + f(P_2)}{2} - f(P_0) = \frac{o_1 + o_2}{2}. \tag{32}$$

By the definition of concave function, it is equivalent to testify the results that Eq. (32) is greater than 0. For the integer $i = 1,2$, o_i is furnished by the Taylor formula, given as

$$\begin{aligned} o_i &= \frac{1}{f_{xx}''}\{[(x_i - x_0)f_{xx}'' + (y_i - y_0)f_{xy}'']^2 + (y_i - y_0)^2[f_{xx}'' \cdot f_{yy}'' - f_{xy}''^2]\} \\ &= \frac{1}{f_{yy}''}\{[(x_i - x_0)f_{xy}'' + (y_i - y_0)f_{yy}'']^2 + (x_i - x_0)^2[f_{xx}'' \cdot f_{yy}'' - f_{xy}''^2]\}. \end{aligned} \tag{33}$$

Note that $f_{xy}''^2 - f_{xx}'' \cdot f_{yy}'' = |\mathbf{H}_C|$. The conclusion may be drawn that $f(x, y)$ would be a concave function if either f_{xx}'' or f_{yy}'' is positive, with the premise $|\mathbf{H}_C| \geq 0$. □

Appendix B

Recalling the Hessian matrix in Eq. (20), the concavity and convexity of binary function $C(\xi, h)$ could be determined with the determinant being positive. As analyzed in the main body of this paper, the prerequisite is to ensure that the second-order partial derivative C_{hh}'' is greater than 0, which is $\frac{2(-1+\xi)[-P_t^2\eta^2R_b\sigma_n^6+3\xi h^4P_t^6\eta^6R_b\sigma_n^2+h^2P_t^4\eta^4(1+\xi)]}{(P_t^2\eta^2h^2+R_b\sigma_n^2)^2(R_b\sigma_n^2+\xi P_t^2\eta^2h^2)^2} \geq 0$.

Consider the h is a parameter, the solution of ξ becomes

$$\xi \in \begin{cases} (-\infty, 1] \cup \left[\frac{-h^2\eta^2P_t^2R_b\sigma_n^2+R_b^2\sigma_n^4}{3h^4\eta^4P_t^4+h^2\eta^2P_t^2R_b\sigma_n^2}, \infty\right), & 0 < h < \sqrt{R_b\sigma_n^2/3P_t^2\eta^2} \\ \left(-\infty, \frac{-h^2\eta^2P_t^2R_b\sigma_n^2+R_b^2\sigma_n^4}{3h^4\eta^4P_t^4+h^2\eta^2P_t^2R_b\sigma_n^2}\right] \cup [1, \infty), & h > \sqrt{R_b\sigma_n^2/3P_t^2\eta^2} \end{cases}. \tag{34}$$

Owing to the hypothesis that $\xi > 0$, it could be obtained that $\xi \in (0,1]$ with h ranging of $0 < h < \sqrt{R_b\sigma_n^2/3P_t^2\eta^2}$.

With the positive h, the solution of $|\mathbf{H}_C| \geq 0$ is deduced as

$$-\frac{R_b\sigma_n^2}{P_t^2h^2\eta^2} < \xi < \frac{R_b^2\sigma_n^4 - 2R_b\sigma_n^2P_t^2h^2\eta^2 - 2P_t^4h^4\eta^4}{R_b\sigma_n^2P_t^2h^2\eta^2 - 2P_t^4h^4\eta^4}. \tag{35}$$

Thus, the span of ξ is supposed to be the intersection of Eqs. (35) and (34). In this way, the function $C(\xi, h)$ becomes a concave one, with ξ ranging from 0 to $\min\left(\frac{R_b^2\sigma_n^4-2R_b\sigma_n^2P_t^2h^2\eta^2-2P_t^4h^4\eta^4}{R_b\sigma_n^2P_t^2h^2\eta^2-2P_t^4h^4\eta^4}, 1\right)$, which may be defined as the "concave scope." In that case, there is extremely tiny probability when ξ is greater than $\min\left(\frac{R_b^2\sigma_n^4-2R_b\sigma_n^2P_t^2h^2\eta^2-2P_t^4h^4\eta^4}{R_b\sigma_n^2P_t^2h^2\eta^2-2P_t^4h^4\eta^4}, 1\right)$, due to the distribution of ξ. For instance, the probability is up to 99.1% lies in the concave scope with the parameters $A = 0.1$, $\sigma = 0.1$. As a result, the conclusion could be drawn that the $C(\xi, h)$ is a concave one with $0 < h < \sqrt{R_b\sigma_n^2/3P_t^2\eta^2}$. However, when $h > \sqrt{R_b\sigma_n^2/3P_t^2\eta^2}$, whether the function is concave or convex still remains uncertain.

Acknowledgments

This work was financially supported by the National Natural Science Foundation of China (NSFC) (No. 51605465).

References

1. M. A. Khalighi and M. Uysal, "Survey on free space optical communication: a communication theory perspective," *IEEE Commun. Surv. Tutorials* **16**(4), 2231–2258 (2014).
2. K. Short et al., "Channel characterization for air-to-ground free-space optical communication links," *Proc. SPIE* **8971**, 897108 (2014).
3. H. A. Willebrand and B. S. Ghuman, "Fiber optics without fiber," *IEEE Spectrum* **38**(8), 40–45 (2001).
4. S. S. Muhammad, P. Kohldorfer, and E. Leitgeb, "Channel modeling for terrestrial free space optical links," in *Proc. of 7th Int. Conf. Transparent Optical Network (ICTON)*, pp. 407–410 (2005).
5. M. A. Al-Habash, L. C. Andrews, and R. L. Phillips, "Mathematical model for the irradiance probability density function of a laser beam propagating through turbulent media," *Opt. Eng.* **40**(8), 1554–1562 (2001).
6. S. Ansari, F. Yilmaz, and M. S. Alouini, "Performance analysis of FSO links over unified gamma-gamma turbulence channels," in *IEEE 81st Vehicular Technology Conf. (VTC Spring)*, Glasgow, pp. 1–5 (2015).
7. H. AlQuwaiee, I. S. Ansari, and M. S. Alouini, "On the performance of free-space optical communication systems over double generalized gamma channel," *IEEE J. Sel. Areas Commun.* **33**(9), 1829–1840 (2015).
8. I. S. Ansari, F. Yilmaz, and M. S. Alouini, "Performance analysis of free-space optical links over mlaga ($\mathcal{M}$) turbulence channels with pointing errors," *IEEE Trans. Wireless Commun.* **15**(1), 91–102 (2016).
9. M. Kashani, M. Uysal, and M. Kavehrad, "A novel statistical channel model for turbulence-induced fading in free-space optical systems," *J. Lightwave Technol.* **33**(11), 2303–2312 (2015).
10. A. Farid and S. Hranilovic, "Outage capacity optimization for free-space optical links withpointing errors," *J. Lightwave Technol.* **25**(7), 1702–1710 (2007).
11. I. S. Ansari, M. S. Alouini, and J. Cheng, "Ergodic capacity analysis of free-space optical links with nonzero boresight pointing errors," *IEEE Trans. Wireless Commun.* **14**(8), 4248–4264 (2015).
12. N. Sharma, A. Bansal, and P. Garg, "Spectrally efficient TWR-aided free-space optical communication over turbulent channel with generalized pointing error," *Trans. Emerg. Telecommun. Technol.* **28**, e3052 (2017).

13. H. AlQuwaiee, H. Yang, and M. S. Alouini, "On the asymptotic capacity of dual-aperture FSO systems with generalized pointing error model," *IEEE Trans. Wireless Commun.* **15**(9), 6502–6512 (2016).
14. R. B. Ruiz et al., "Outage performance of exponentiated Weibull FSO links under generalized pointing errors," *J. Lightwave Technol.* **35**(9), 1605–1613 (2017).
15. J. Wang et al., "Outage analysis for relay-aided free-space optical communications over turbulence channels with nonzero boresight pointing errors," *IEEE Photonics J.* **6**(4), 1–9 (2014).
16. X. M. Zhu and J. M. Kahn, "Free-space optical communication through atomospheric turbulence channels," *IEEE Trans. Commun.* **50**(8), 1293–1300 (2002).
17. M. Jarzyna, P. Kuszaj, and K. Banaszek, "Incoherent on-off keying with classical and non-classical light," *Opt. Express* **23**(3), 3170–3175 (2015).
18. S. Cui et al., "Improved symbol rate identification method for on-off keying and advanced modulation format signals based on asynchronous delayed sampling," *Opt. Commun.* **354**(1), 218–224 (2015).
19. K. Kiasaleh, "Receiver architecture for channel-aided, OOK, APD-based FSO communications through turbulent atmosphere," *IEEE Trans. Commun.* **63**(1), 186–194 (2015).
20. C. E. Shannon, "Communication in the presence of noise," *Proc. IRE* **37**(1), 10–21 (1949).
21. K. P. Peppas et al., "Capacity analysis of dual amplify-and-forward relayed free-space optical communication systems over turbulence channels with pointing errors," *J. Opt. Commun. Networking* **5**, 1032–1042 (2013).
22. R. B. Ruiz et al., "On the capacity of MISO FSO systems over gamma-gamma and misalignment fading channels," *Opt. Express* **23**(17), 22371–22385 (2015).
23. H. Wang, X. Wang, and M. Cao, "Ergodic channel capacity of spatial correlated multiple-input multiple-output free space optical links using multipulse pulse-position modulation," *Opt. Eng.* **56**(2), 026103 (2017).
24. J. Park et al., "Outage probability analysis of a coherent FSO amplify-and-forward relaying system," *IEEE Photonics Technol. Lett.* **27**(11), 1204–1207 (2015).
25. D. Shah, D. Kothari, and A. Ghosh, "Performance of free-space optical link with wavelength diversity over exponentiated Weibull channel," *Opt. Eng.* **55**(11), 116112 (2016).
26. N. Ou et al., "Jitter models for the design and test of Gbps-speed serial interconnects," *IEEE Des. Test Comput.* **21**(4), 302–313 (2004).
27. K. M. N. Islam and S. P. Majumder, "Effect of timing jitter on the BER performance of a *M*-PPM FSO link over atmospheric turbulence channel," in *IEEE 8th Int. Conf. on Electrical and Computer Engineering*, pp. 409–412, Dhaka, Bangladesh (2014).
28. Y. Wang et al., "The influence of timing error on the performance of optical pulse PPM system in atmospheric turbulent channels," in *IEEE Symp. Photonics and Optoelectronics.*, pp. 1–4, Chengdu, China (2010).
29. Y. Li et al., "Timing jitter's influence on the symbol error rate performance of the *L*-ary pulse position modulation free-space optical link in atmospheric turbulent channels with pointing errors," *Opt. Eng.* **56**(3), 036116 (2017).
30. L. Yang, X. Gao, and M.-S. Alouini, "Performance analysis of relay-assisted all-optical FSO networks over strong atmospheric turbulence channels with pointing errors," *J. Lightwave Technol.* **32**(23), 4613–4620 (2014).
31. J. B. Wang et al., "Tight bounds on channel capacity for dimmable visible light communications," *J. Lightwave Technol.* **31**(23), 3771–3779 (2013).
32. V. S. Aadamchik and O. I. Marichev, "Algorithm for calculating integrals of hypergeometric type functions and its realization in reduce system," in *ISSAC 90 Proc. Int. Symp. on Symbolic and Algebraic Computation*, pp. 212–224, Tokyo, Japan (1990).

Yatian Li received his BS and MS degrees (with hons) in communications engineering from Harbin Institute of Technology (HIT), Harbin, China, in 2013 and 2015, respectively. Currently, he is pursuing his PhD in mechanical electrical engineering at the University of Chinese Academy of Sciences (UCAS), Beijing, China. He is a research assistant at Changchun Institute of Optics, Fine Mechanics and Physics (CIOMP), Chinese Academy of Sciences, Changchun, China. His current research interests include free space optics and wireless communications.

Shaoai Guo received her BS degree (with hons) in electronic and information engineering from Jilin University (JLU), Changchun, China, in 2013, and her MS degree in electronic circuits and systems from the UCAS, Beijing, China, in 2016. She served as a research assistant at Chang Guang Satellite Technology Co., Ltd., Changchun, China. Her current research interests include satellite communications and wireless communications.

Tianwen Geng received his BS and MS degrees in electronic circuits and systems from JLU, Changchun, China, in 2004 and 2007, respectively. He is an associate researcher at CIOMP, Chinese Academy of Sciences, Changchun, China.

Shuang Ma received his BS degree in optical information engineering from JLU, Changchun, China, in 2010, and his PhD in electronic circuits and systems from the UCAS, Beijing, China, in 2016. He is a research assistant at CIOMP, Chinese Academy of Sciences, Changchun, China.

Shijie Gao received his BS degree in mechanical electrical engineering from Harbin University of Science and Technology (HUST), Harbin, China, in 2010, and his MS and PhD degrees in electronic circuits and systems from the UCAS, Beijing, China, in 2006 and 2015, respectively. He is an associate researcher at CIOMP, Chinese Academy of Sciences, Changchun, China.

Huibin Gao received his BS and MS degrees from Jilin University of Technology, Changchun, China, in 1985 and 1990, respectively. He has published more than 50 papers in journals and conferences. He is a full researcher at CIOMP, Chinese Academy of Sciences, Changchun, China. His current research interests include autocontrol and servo trace technology.